Master of
Science Thesis
VT2019

Optimization of dose in relation to image quality in synchrotron based tomographic lung-imaging

---

Sajad Mohammed Ali

Supervision

Rajmund Mokso

Department of Medical Radiation Physics,
Clinical Sciences, Lund
Lund University

Popular summary in Swedish

Populärvetenskaplig beskrivning

Bildgivning av lungor har länge varit och är än ett viktigt forskningsområde eftersom lungkomplikationer är en stor anledning till sjuklighet och dödlighet över hela världen. Med den fortsatta forskningen och de förbättrade avbildningarna ökar kunskapen, vilken bidrar till förbättrad sjukvård. I dagsläget utförs en stor mängd lungavbildningar med *synkrotronljuskällor*. Dessa är ljusstarka röntgenkällor som ger möjlighet till att producera högupplösta avbildningar med mycket hög bildkvalitet i förhållande till ordinarie lung-röntgenavbildningar som utförs inom bland annat sjukvården. I dagsläget är lungavbildningar med synkrotronljuskällor fortfarande i ett prekliniskt stadie och samtliga avbildningar görs på gnagare och andra representativa djur. Det är i förstahand tomografiska bilder som skapas, vilka är snittade bilder av hela den undersökta volymen. Vid insamling av tomografiska bilder med synkrotronljuskällor roteras den undersökta volymen i samband med att strålningen inkommer. För att få en avbildning med god bildkvalitet måste en stor mängd vinklar bestrålas, ju fler desto bättre bildkvalitet, normalt bestrålas omkring 900 vinklar. En större mängd bestrålade vinkar innebär däremot även att strålningsdosen till objektet blir högre. Syftet med denna studie var således att undersöka om det finns ett optimalt antal projektionsvinklar att bestråla för att få så hög bildkvalitet som möjligt till så låg kostnad av absorberad dos till det undersökta objektet som möjligt. En mindre utredning om huruvida lungavbildning baserad på fasskiftet av röntgenstrålningen ger bättre kontrast än avbildning baserad på absorptionen av röntgenstrålningen var också ämnad att göras inom ramen för denna studie.

Resultatet från jämförelsen mellan bilderna från fasskifte respektive absorption visade entydigt på att bilderna genererade med fasskifte hade åtminstone 18 gånger bättre bildkvalitet. Utifrån analysen av det producerade undersökningsmaterialet för den egentliga frågeställningen, upptäcktes att det inte finns ett entydigt värde på antal projektionsvinklar som är optimalt för att maximera bildkvaliteten samtidigt som dosen till objektet minimeras. Det upptäcktes att det uppstår en platå när man fortsätter att minska antalet projektionsvinklar under 400. Det innebär att det finns flera antal projektionsvinklar som optimerar bildkvaliteten i förhållande till den absorberade dosen i objektet. Det kan konstateras från upptäckten att vid användning av upp till 400 projektionsvinklar får man ”mest bildkvalitet för den absorberade dosen”. Däremot kan det inom ramen för denna studie inte avgöras om alla dessa bilder är användbara. Den ena anledningen är att det finns flera andra mått på bildkvalitet, såsom upplösning, som inte berörs i denna studie. Den andra och viktigaste anledningen till att användbarheten av dessa bilder inte kan avgöras är att lung-bilder genererade med synkrotronljuskällor förutsätter möjligheten till binärisering (bilden behandlas så att det som syns antigen är luft eller alveoler) för att kunna analyseras. Resultatet från den utförda studien sätter alltså ramen för en ny studie i syfte att besvara frågeställningen om huruvida det är möjligt att binärisera alla (eller någon av) bilderna genererade med upp till 400 projektionsvinklar.

Abstract

Introduction: Lung imaging with synchrotron light sources is currently a widely studied field. The image resolution and quality are remarkable and the level of detail possible to study the smallest structures, the alveoli, of the lungs cannot be obtained by any other non-invasive imaging modality with the current technology. The most common and useful type of lung imaging with brilliant light sources is tomographic imaging which is being performed exclusively on rodents at the current state. However, in the case of tomographic imaging with synchrotron light sources the absorbed doses to the samples are high due to the high photon flux. Although exposure times don't extend a few milliseconds the number of irradiated angles is normally in the order of 900. Thus, the main objective was to investigate whether there is an optimal number of projection angles that should be used in order to maximize image quality while simultaneously minimizing the dose to the sample i.e. maximize the image quality-to-dose ratio. A subobjective of the study was to investigate the improvement of image quality when generating phase contrast images compared to standard absorption contrast images.

Materials and Methods: A tomographic acquisition of static mouse lungs were performed at the TOMCAT beamline of SLS. In the frameworks of Python, the data was reconstructed with all projections (900) using two different reconstruction algorithms, Gridrec and SIRT. For the investigation of the subobjective the data was reconstructed, by both algorithms, with and without the application of a phase retrieval algorithm. The main investigation was done by generating 8 images with each reconstruction algorithm. The images were generated with a decreasing number of projection angles. The first included all the projection angles, the second kept only every other projection, the third kept every third etc. Thus, the number of used projection angles for the 8 images were 900, 450, 300, 225, 180, 150, 128 and 112 respectively. ESD was used as dose concept and *CNR* as a measure of image quality. The theoretical ESD was calculated for the images with different number of projection angles and *CNR*. Finally, the *CNR*-ESD ratio was determined.

Results: As Kitchen et. al. (2017) suggests it could be seen that the image quality was greatly improved with the application of phase retrieval to generate phase contrast images in comparison to standard AC-images. This was the case when using both the Gridrec and SIRT algorithms for reconstruction as the CNR was at least 18 times better in the phase contrast images. It was found that there is not one optimal number of projection angles for the image quality-to-dose ratio but rather that a plateau appears from approximately 400 projection angles in the direction of decreasing number of projections.

Discussion and conclusion: The results of the subobjective were straightforward concluding that phase contrast is advantageous over absorption contrast in relation to image quality when probing with synchrotron light sources (with monochromatized X-rays) although, the improvement in image quality varies somewhat depending on what reconstruction algorithm is used since the phase retrieval algorithm is integrated into the reconstruction. While the gain in image quality-to-dose ratio is the highest over the whole plateau region, it must be taken into consideration that *CNR* is not the only metric for image quality. The resolution also degrades as the dose is decreased. More importantly in the field of lung imaging the images must be capable of being segmented (binarized, between tissue and air) which might be a problem when going to the low part of the plateau. While it has been discovered that a plateau appears for the image quality-to-dose ratio as the number of angles are decreased it must be concluded that further investigation must be carried out, especially testing the possibility of segmenting the images with decreased number of projection, in order to determine whether these are usable or not.

Abbreviations

AC – Absorption contrast

CMOS – Complementary Metal Oxide Semiconductor

CNR – Contrast to noise ratio

CT – Computed tomography

ESD – Entrance skin dose

FBP – Filtered back projection

FoV – Field of view

FST – Fourier Slice Theorem

PR – Phase retrieval

ROI – Region of interest

SD – standard deviation

SIRT – Simultaneous Iterative Reconstruction Technique

SLS – Swiss light source

Contents

1. Introduction

In recent years multiple studies e.g. [1], [2] and [3] have been conducted within the field of lung imaging using brilliant light sources such as third generation synchrotron light sources. With such light sources the possibility of probing structures down to the order of microns, in some cases even to the order of nanometers, [7] are possible. Thus, imaging the smallest structures of the lung i.e. the alveoli (figure 1) is possible which in tur opens a wide field for better understanding both anatomy and physiology of these structures and the lung as a unit. The understanding is of importance to improve the clinical knowledge given that lung complications represent a vast part of worldwide morbidity and mortality. [3]

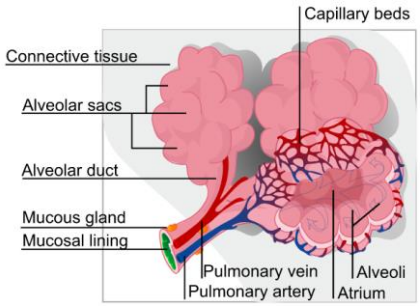

Figure 1. An illustration of the anatomy of human alveoli, i.e. the smallest structures of the lung. [14]

Nevertheless, the detailed studies of the alveoli with brilliant light sources are still at a preclinical state and exclusively carried out on rodents and other representative animals. Three-dimensional lung images of animal lungs have been acquired in large sets. Also, four dimensional images have been collected adding *time* as the fourth dimension when probing dynamic lungs. Special reconstruction algorithms have been developed for such purposes [4]. However, using brilliant light sources for probing structures have limitations since radiation damage on the sample will be a fact as the irradiations are prolonged and thus the doses increased. This in turn limits the resolution [6]. While there are methods being developed to decrease the doses to the sample while maintain the resolution, such as using phase retrieval algorithms (Paganin et al) which have been studied in [1], the radiation damage cannot be precluded entirely and the doses are yet rather high. This is particularly the case when tomographic images are acquired since a large number of projection angles are required. In contrast, if the number of projection angles are decreased the dose to the sample decreases as does the image quality. As such the main objective of this study have been to investigate the limits, dose puts to image quality when acquiring tomographic data. In particular the goal is to investigate whether there is an optimal number of projection angles in relation to both dose and image quality when acquiring a tomographic image. In order to create a framework for this evaluation a set of subobjectives have been carried out prior to the main investigation. Including the measurement of improvement in image quality when using a phase retrieval algorithm as has been done in [1] and using different reconstruction algorithms.

2. Theory

2.1 Tomographic reconstruction

Imaging a 3D – volume as a set of slices is referred to as tomography. Each tomographic slice can be created by first projecting the object with some probing medium e.g. X-rays at several angles over an interval of 180 degrees. The signal variation in each of the projections, as registered in the detectors behind the object, will be due to attenuation differences in the object (figure 2). The slices can then be reconstructed by back projecting the signal data from all projections with different methods. [8]

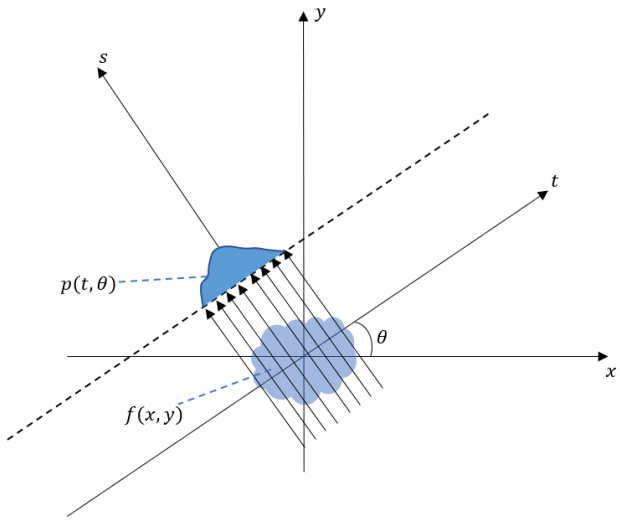

Figure 2. The projection $p(t,\theta)$ of the object function $f(x,y)$ at the angle θ.

The projections $p(t,\theta)$ of an object $f(x,y)$ are expressed mathematically with the Radon transform as follows:

$$R\{f(x,y)\} = p(t,\theta) = \int_{-\infty}^{\infty} f(x,y)\, ds \quad (1)$$

The relations between the two coordinate systems seen in figure 2 can be expressed by the following four equations:

$$x = t \cdot \cos\theta - s \cdot \sin\theta \quad (2)$$
$$y = s \cdot \cos\theta + t \cdot \sin\theta \quad (3)$$
$$t = x \cdot \cos\theta + y \cdot \sin\theta \quad (4)$$
$$s = -x \cdot \sin\theta + y \cdot \cos\theta \quad (5)$$

Insertion of equations (2) – (3) gives the extended expression of the Radon transformation of the object function, with the same variables as the integrand:

$$R\{f(x,y)\} = \int_{-\infty}^{\infty} f(t \cdot \cos\theta - s \cdot \sin\theta\,, s \cdot \cos\theta + t \cdot \sin\theta)\, ds \quad (6)$$

By taking the Fourier transform the following is obtained:

$$F\{R\{f(x,y)\}\} = \int_{-\infty}^{\infty} \left\{ \int_{-\infty}^{\infty} f(t \cdot \cos\theta - s \cdot \sin\theta\,, s \cdot \cos\theta + t \cdot \sin\theta)\, ds \right\} e^{-2\pi i \tau t}\, dt \quad (7)$$

With the insertion of equations (4) – (5) and variable change of the integrands:

$$F\{p(t,\theta)\} = \int_{-\infty}^{\infty} \int_{-\infty}^{\infty} f(x,y) e^{-2\pi i \tau (x \cdot \cos\theta + y \cdot \sin\theta)} dx dy = F(\tau\cos\theta\,, \tau\sin\theta) \quad (8)$$

It can thus be concluded that the Fourier transform of the projections gives a profile through origin in the angle θ for the object function in the Fourier space. This is referred to as the *Fourier slice theorem*

In order to reobtain the object function $f(x,y)$ from its Fourier transform $F(u,v)$ a simple invers Fourier transform is required:

$$f(x,y) = F^{-1}\{F(u,v)\} = \iint F(u,v) e^{2\pi i (xu + yv)}\, du dv \quad (9)$$

Introducing the following variable substitution:

$$u = \tau \cos\theta$$
$$v = \tau \sin\theta$$
$$dudv = \tau \, d\tau d\theta$$

Equation (9) becomes:

$$f(x,y) = \iint F(\tau\cos\theta\,, \tau\sin\theta) e^{2\pi i(x\tau\cos\theta + y\tau\sin\theta)} \, \tau \, d\tau d\theta \quad (10)$$

Since a back projection in 360 degrees is required to reproduce the image, the mirror of the 180-degree projections $p(t,\theta)$ is required which is simply $p(t,\theta+\pi)$. This must be added to equation (10) so that the back projection covers the whole 360 degrees. Since the following trigonometrical relation applies:

$$\sin(\theta+\pi) = -\sin\theta$$
$$\cos(\theta+\pi) = -\cos\theta$$

The addition of the mirroring projections to equation (10) gives:

$$f(x,y) = \int_0^{\pi}\int_0^{\infty} F(\tau\cos\theta\,, \tau\sin\theta) e^{2\pi i(x\tau\cos\theta + y\tau\sin\theta)} |\tau| d\tau d\theta \quad (11)$$

From the Fourier slice theorem and equation (4) equation (11) can be rewritten:

$$f(x,y) = \int_0^{\pi}\int_0^{\infty} (F\{p(t,\theta)\}|\tau|) e^{2\pi i t\tau} d\tau d\theta \quad (12)$$

The interpretation of equation (12) is that the image $f(x,y)$ is reobtained if the Fourier transform of the projections $F\{p(t,\theta)\}$, which in accordance with FST gives a slice in the angle θ in the Fourier space, is multiplied by a filter term $|\tau|$ before being inverse transformed and then back projected over the interval $0-\pi$. The process is often referred to as the standard FBP process. In the terms of the back-projection operator $B\{\ \ \}$ and Fourier transform operator $F\{\ \ \}$ equation (12) is written as:

$$f(x,y) = B\{F^{-1}\{F\{p(t,\theta)\} \cdot |\tau|\}\} (13)$$

In the case of tomographic imaging with synchrotron light, the incident light from the beamline probes the object while the object is being rotated, i.e. while the angle is being varied. Normally the number of projection angles are in the order of 900. The images are often reconstructed by one of the following algorithms *Gridrec* and *SIRT*.

2.1.1 Gridrec

The Gridrec reconstruction algorithm is based on the standard FBP method which is described in section 2.1. By sampling the discretized Fourier transform of the projections, i.e. the signal data in the Fourier space, in predefined grids before back projecting the reconstruction process is accelerated.

2.1.2 SIRT

Each projection can be expressed as the real image being forward projected by the scanning process. This can in turn be expressed in terms of a linear equation. As such the projections of the whole object can be expressed as a system of linear equations:

$$\boldsymbol{Ax} = \boldsymbol{b} \ (14)$$

where $\boldsymbol{A}$ is the scanning process, $\boldsymbol{x}$ the image and $\boldsymbol{b}$ the measured projections. The system is solved by minimizing:

$$|\boldsymbol{Ax} - \boldsymbol{b}| \ (15)$$

Which is what different reconstruction algorithm does. In the case of the SIRT algorithm this is done by firstly forward projecting the current image $\boldsymbol{x}^{(n)}$ and subtracting this term from the real projections $\boldsymbol{b}$:

$$\left(\boldsymbol{b} - \boldsymbol{Ax}^{(n)}\right) (16)$$

The difference is then back projected into the reconstruction field by multiplication with the transposed matrix of the scanning process $\boldsymbol{A^T}$ weighted with the matrices $\boldsymbol{C}$ and $\boldsymbol{R}$:

$$\boldsymbol{CA^TR}\left(\boldsymbol{b}-\boldsymbol{Ax}^{(n)}\right) \quad (17)$$

Where the weighting matrices $\boldsymbol{C}$ and $\boldsymbol{R}$ are diagonal matrices that contain the inverse sum of the columns and rows of scanning process matrix $\boldsymbol{A}$ respectively:

$$c_{jj} = \frac{1}{\sum_i a_{ij}} \quad r_{jj} = \frac{1}{\sum_j a_{ij}} \quad (18)$$

The correction term as given in equation (17) is then added to the current image giving the new image:

$$\boldsymbol{x}^{(n+1)} = \boldsymbol{x}^{(n)} + \boldsymbol{CA^TR}\left(\boldsymbol{b}-\boldsymbol{Ax}^{(n)}\right) \quad (19)$$

The process is then repeated each repetition is one iteration. [9]

2.2 Phase Retrieval

In traditional X-ray tomographic imaging, for example within the medical field with CT, the image contrast relies on absorption. However, the refractive index n of an object can be expressed as:

$$n = 1 - \delta + \beta i \quad (20)$$

Where the complex part, β describes the absorption in the material while the real part δ describes the phase shift caused by the probed medium [10]. Thus, in traditional X-ray imaging the contrast is due to the imaginary part. Consequently, the contrast of the image can be generated by considering the real part of equation (20) i.e. the contrast can be generated by considering the phase shift, intensity variations, that the medium causes by scattering the X-rays. There are several methods used to generate phase contrast [11] however, the most advantageous and simples arranged method is the in-line phase contrast (also called propagation-based phase contrast). This method relies on the propagation of the X-rays after

interacting with the probed medium. With the correct propagation distance, the registered intensity can be greatly enhanced especially at the edges of structures on the probed medium. Consequently, the method requires highly monochromatic X-rays, as such the method is very suitable for images generated by synchrotron light sources. [10, 11]

The phase contrast methods cannot generate direct measurements of the phase. Therefore, computational data processing is required. For the in-line phase contrast method phase retrieval is required. There are various methods for solving this problem, however all the methods follow the same pattern which mathematically can be expressed as:

$$\phi(\mathrm{r}\perp) = f\left(F^{-1}\left\{H_p \cdot F\{g(I)\}\right\}\right) \quad (21)$$

The interpretation is that a phase function $\phi(\mathrm{r}\perp)$ is obtained by first taking the Fourier transform of a function of the measured intensity $F\{g(I)\}$ and multiplying with a filter H_p in the Fourier space. The product is then inverse Fourier transformed and the phase function obtained.

When the phase function has been obtained a reconstruction must be done in order to get a phase contrast image. This can be done by any reconstruction algorithm. In the case of FBP, equation (13), the phase function $\phi(\mathrm{r}\perp)$ is first Fourier transformed. The Fourier transform of the phase function is then multiplied with a FBP-filter $|\tau|$ in the Fourier space. The next step is inverse Fourier transform of the product and finally a back projection giving a phase contrast image $f_{PR}(x, y)$:

$$f_{PR}(x, y) = B\left\{F^{-1}\{F\{\phi(\mathrm{r}\perp)\} \cdot |\tau|\}\right\} \quad (22)$$

2.3 Dose Calculation

Absorbed dose D is defined as the mean energy imparted from ionizing radiation per unit mass. In the case of photons, the energy imparted to the electrons contributing to ionization in the medium is considered. [12]

$$D = \frac{E_{imp}}{m} \quad (23)$$

The SI-unit for the absorbed dose is Joules per kg, also referred to as gray (Gy). [12] A simplifying approximation can be made that the irradiated medium is homogenous and the probing X-rays monochromatic with the energy $h\nu$. With *Beer Lambert's law* the number of absorbed photons in the medium ΔI can be expressed as:

$$\Delta I = I_0 - I = I_0 - I_0 e^{-\frac{\mu_{en}}{\rho}\rho\Delta x} \quad (24)$$

Where I_0 is the number of incident photons, μ_{en}/ρ the mass absorption coefficient, ρ the density and Δx the depth of the medium. Equation (23) can then be rewritten:

$$D = \frac{\Delta I \cdot h\nu}{m} = \frac{I_0\left(1 - e^{-\frac{\mu_{en}}{\rho}\rho\Delta x}\right)h\nu}{m} \quad (25)$$

Another commonly used dose concept is the *Entrance Skin Dose* (ESD) which considers the dose to the outermost surface of the irradiated medium. An expression for the ESD can easily be derived form equation (25).

By rewriting m in terms of volume, equation (25) becomes:

$$D = \frac{I_0\left(1 - e^{-\frac{\mu_{en}}{\rho}\rho\Delta x}\right)h\nu}{V\rho} = \frac{I_0\left(1 - e^{-\frac{\mu_{en}}{\rho}\rho\Delta x}\right)h\nu}{A\Delta x\rho} \quad (26)$$

Where A is the cross section of the irradiated medium and Δx the depth as earlier stated. By making the following substitution, $y = -\mu_{en} \cdot \Delta x$, equation (26) becomes:

$$D = \frac{I_0}{A} \cdot \frac{(e^y - 1)}{y}\left(\frac{\mu_{en}}{\rho}\right)h\nu \quad (27)$$

To determine the dose to the outermost surface, the depth of the medium is going towards 0 $\Delta x \to 0$. From the earlier made substitution it follows that $y \to 0$. Equation (27) then becomes:

$$ESD = \lim_{y\to 0} \frac{I_0}{A} \cdot \underbrace{\frac{(e^y - 1)}{y}}_{=1}\left(\frac{\mu_{en}}{\rho}\right)h\nu = N\left(\frac{\mu_{en}}{\rho}\right)h\nu \quad (28)$$

Where N is the number of incident photons per surface area. This term is expressed in the same unit as $1/\mu_{en}^2$. Thus, equation (28) is often rewritten as the following [4, 14]:

$$ESD\ [\mathrm{Gy}] = 1.602 \cdot 10^{-4} \cdot \frac{I_0[\mathrm{photons/\mu m^2}] \cdot h\nu[\mathrm{eV}]}{\mu^{-1}[\mathrm{\mu m}] \cdot \rho[\mathrm{g/cm^3}]} \quad (29)$$

2.4 Image quality

In the field of lung imaging with brilliant light sources an often-used measure of image quality is CNR because the visible structures in the images are either tissue (alveoli) or surrounding air. The large difference between the mean-signal-values of tissue and air makes *CNR* suitable. In order to determine the CNR of an image a *ROI* is placed over a uniform region of the first structure giving a mean value of the signal S_1within and the standard deviation of the region SD_1. Another ROI is placed over a homogenous region of the second structure, or background, from which the mean signal value S_2 and standard deviation SD_2 are given. This is illustrated in figure 3.

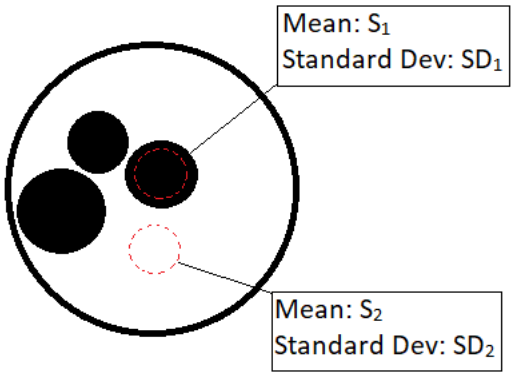

Figure 3. An illustration of the placement of regions of interest in the different regions of an image in order to determine the CNR.

The CNR can then be calculated by taking the absolute value of the difference of the signal values divided by the square root of the quadratic sum of the standard deviations of the two regions.

$$CNR = \frac{|S_1 - S_2|}{\sqrt{SD_1^2 + SD_2^2}} \quad (30)$$

Where S_1, S_2, SD_1 and SD_2 are the mean values and standard deviations of regions 1 and 2 respectively.

3. Materials and methods

3.1 Image acquisition

The experimental setup, at the X02DA TOMCAT beamline of SLS, for the acquisition of the tomographic lung images is illustrated in figure 4. An adult Balb-C mouse was prepared for postmortem imaging by being given anesthesia and an overdose of *pentobarbital* in order to avoid heartbeat causing motion artefacts. The preparation and execution of the experiment was approved and supervised by the Swiss Agency for the Environment, Forest and Landscape and the veterinary service of the Canton of Bern.

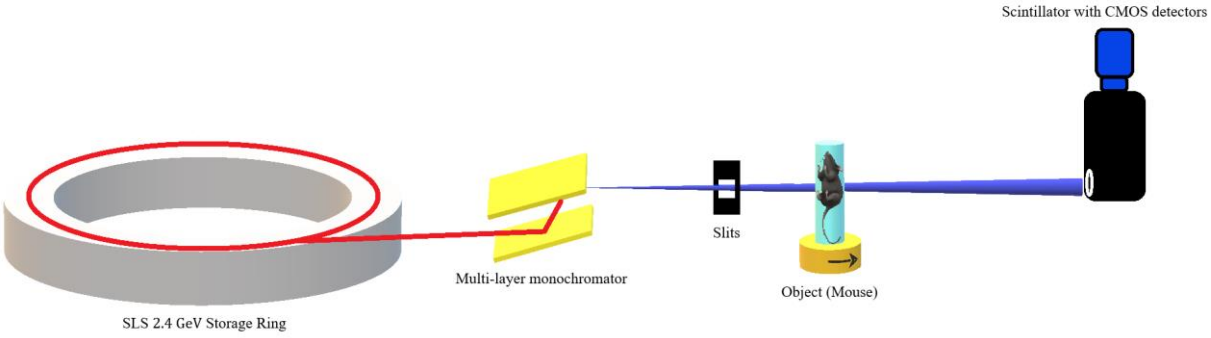

Figure 4. The experimental setup for the image acquisition.

The mouse was placed in an upright position by a custom-made holder placed on top of a rotatable table in the field of view of the beam. The X-ray beam was generated from a 2.4 GeV storage ring with a 2.9 T bending magnet. The beam energy was tuned to 22 keV by being monochromatized with a multi-layer monochromator. The propagation distance was set to 10 cm. A set of CMOS detectors coupled to a scintillator were used with pixel size of 3 μm. The photon flux was set to $7 \cdot 10^4$ photons/s/µm^2 and the exposure time to 2 ms. The number of projected angles were 900 over an interval of 180 degrees.

3.2 Data processing and analysis

After the acquisition of the tomographic data all the required work to be done for the main and subobjectives were computational. On one hand phase retrieving and reconstructing the tomographic data with the Gridrec and SIRT reconstruction algorithms, all this through coding in Python making use of existing reconstruction modules. On the other hand, analyzing the reconstructed images in ImageJ and through ROI-analysis determine the CNR-of all generated images. All the computational work was executed in the cluster of *MAX-IV*. The codes were written and executed in both *Jupyter Notebook* and *Spyder*. The codes are available as

Notebooks at https://www.kaggle.com/sajadma/tomorec-lungs (reconstructions, phase retrieval etc.) and at https://www.kaggle.com/sajadma/dose-calculations (calculations).

3.2.1 Preparations and reconstruction

In the framework of Python, a package named *Tomopy* was used for reconstruction and phase retrieving of the acquired tomographic data. However, regardless of which of the two reconstruction algorithms was intended to be used a number of preparations had to be done to the tomographic data prior to reconstruction. These lines as coded are shown in figure 5

```
theta = tomopy.angles(proj.shape[0])
```

```
proj = tomopy.normalize(proj, flat, dark)
print(proj.shape)
```

```
(901, 1048, 2016)
```

```
rot_center = tomopy.find_center(proj, theta, init=1008, ind=0, tol=0.5)
print(rot_center)
```

```
[1002.4875]
```

```
proj = tomopy.minus_log(proj)
```

Figure 5. Some of the necessary preparational computations executed on the tomographic data prior to reconstruction.

In the first line the 900 projection angles of the tomographic data are evenly distributed over an interval of 180 degrees. The second line shows that the tomographic data was normalized, the used module takes the signal values of the projections and subtracts with the signal due to detector noise and then divides by the signal when no object is projected subtracted by detector noise. In the third line the rotation center for reconstruction is determined and the last line takes the negative logarithm of the projections.

Another preparation that was done to the tomographic data prior to reconstruction was application of padding in order to remove the gradient around the FoV. The code is shown in figure 6. It should be noted that a new rotation center was defined (last line in figure 6) since the matrix size was changed.

```
N = proj.shape[2]
proj_pad = np.zeros([proj.shape[0],proj.shape[1],3*N//2],dtype = "float32")
proj_pad[:,:,N//4:5*N//4] = proj
proj_pad[:,:,0:N//4] = np.tile(np.reshape(proj[:,:,0],[proj.shape[0],proj.shape[1],1]),(1,1,N//4))
proj_pad[:,:,5*N//4:] = np.tile(np.reshape(proj[:,:,-1],[proj.shape[0],proj.shape[1],1]),(1,1,N//4))

proj = proj_pad
rot_center = rot_center+N//4
```

Figure 6. Code for padding the tomographic data to remove gradient around the FoV.

The padding was only applied when the intention was to reconstruct with Gridrec. Padding to remove the gradient around the FoV when reconstructing with the SIRT algorithm did not give the desired outcome and was therefore neglected.

The last preparation refers only to the SIRT-reconstruction. Since the SIRT algorithm is an iterative reconstruction method (described in section 2.1.2) the suitable amount of iterations for reconstructing the tomographic images had to be determined. To do so one slice of the tomographic data was reconstructed by SIRT with 50, 100, 150, 200 and 300 iterations. The image quality (*CNR*) was calculated and compared for the images with different number of iterations from which it was clear that the 300-iteration image was the most suitable for the remaining investigations. Thus, from this point on into the study every time a reconstruction by SIRT was intended 300 iterations were used.

3.2.2 Phase retrieval

After all the preparations described in section 3.2.1 were done. One slice from the tomographic data was reconstructed with all the projections (900) by both the Gridrec and SIRT algorithms generating typical attenuation contrast images. In the next step the non-reconstructed tomographic data was subjected to phase retrieval by the method of Paganin et al. [14]. In the Tomopy package there's a specially developed module for this which was used as shown in figure 7.

```
proj=tomopy.prep.phase.retrieve_phase(proj,pixel_size=0.0003,dist=10,energy=22,alpha=0.00005,pad=True)
```

Figure 7. The module for phase retrieval by the method of Paganin et al. [14]

As can be seen in the code the phase retrieval module requires information about propagation distance, pixel size, photon energy and an additional term named *alpha* which is the ratio of the complex and real parts of the refractive index of the material, equation (20). Since these parameters are all know they were inserted into the module. However, after phase retrieving a number of slices it was seen that the phase contrast was not optimal. Therefore, the alpha parameter was tweaked several times until the optimal phase contrast was found. Then the same slice as above (with all the 900 projections) was reconstructed with the addition of phase retrieval and by both Gridrec and SIRT.

The CNR of the four generated images was calculated using equation (30). The values of the variables for the calculation were obtained by ROI- analysis with ImageJ as described in section 2.4.

3.2.3 Main investigation

In the second part, the main investigation, eight phase contrast images (the same slice) were generated with each reconstruction algorithm. The number of projection angles was varied between the eight images. The first image included all projection angles when being reconstructed, for the second image every other projection angle was kept, for the third every third projection was kept etc. Thus, the number of used projection angles for the eight images varied as 900, 450, 300, 225, 180, 150 and 112.

The images were then subjected to analysis in ImageJ. To determine the mean signal values and standard deviations for the CNR calculation, equation (30), the ROIs of regions 1 and 2 were placed on the same coordinates for all the images respectively in order to increase consistency of the measurements. After obtaining the necessary values the CNR was calculated according to equation (30). A calculation of ESD to the object as the number of projection angles was varied was done using equation (29). Finally, the ratio of the CNR and the dose (ESD) was calculated for all images and plotted as a function of the number of projection angles.

4. Results

4.1 PR compared to AC

Figure 8 shows one slice of the acquired dataset reconstructed with Gridrec and all projection angles (900). The left image is a standard attenuation contrast image while the right image has been treated with phase retrieval before reconstruction generating a phase contrast image. Figure 9 shows the corresponding slices reconstructed with the SIRT-algorithm. The ESD to the mouse-sample was $21.0\ \mathrm{Gy}$ for all images generated with 900 projection angles, as calculated by equation (29), regardless of what reconstruction algorithm was used and if phase retrieval was applied or not. This is because both reconstruction and the phase retrieval are post-acquisition processes and thus don't affect the dose to the sample. The CNR was 1.1 and 32.6 for the AC respectively the PR images of the Gridrec reconstruction. While it was 1.07 and 18.2 for the AC respectively the PR images of the SIRT reconstruction.

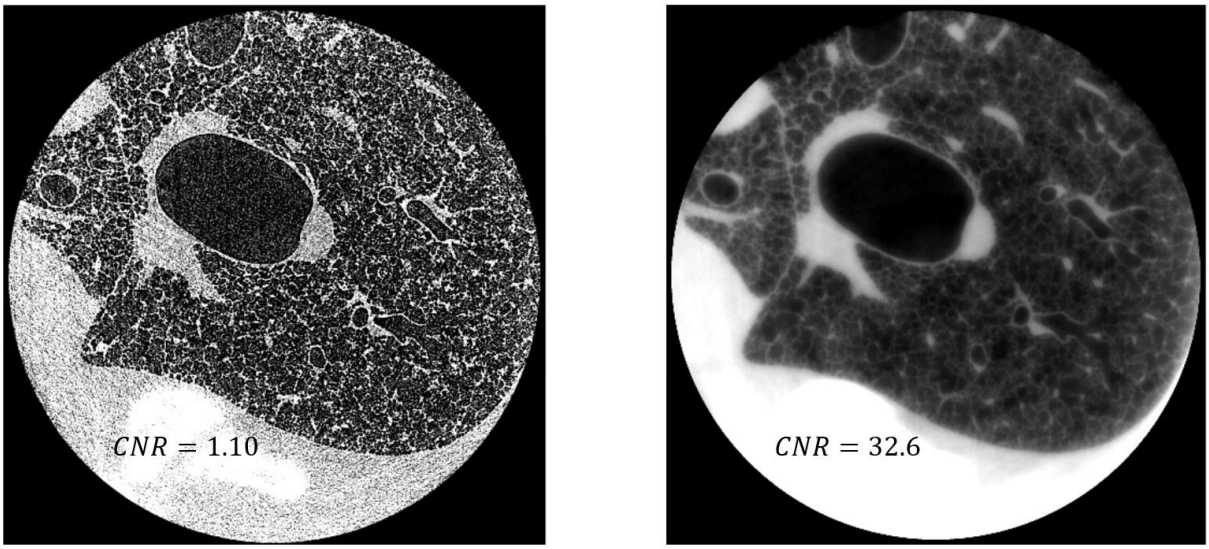

Figure 8. a) One tomographic slice with attenuation contrast reconstructed with the Gridrec algorithm and b) the same slice treated with phase retrieval before reconstruction. The CNR of the AC-image is 1.1 and of the PR image 32.6

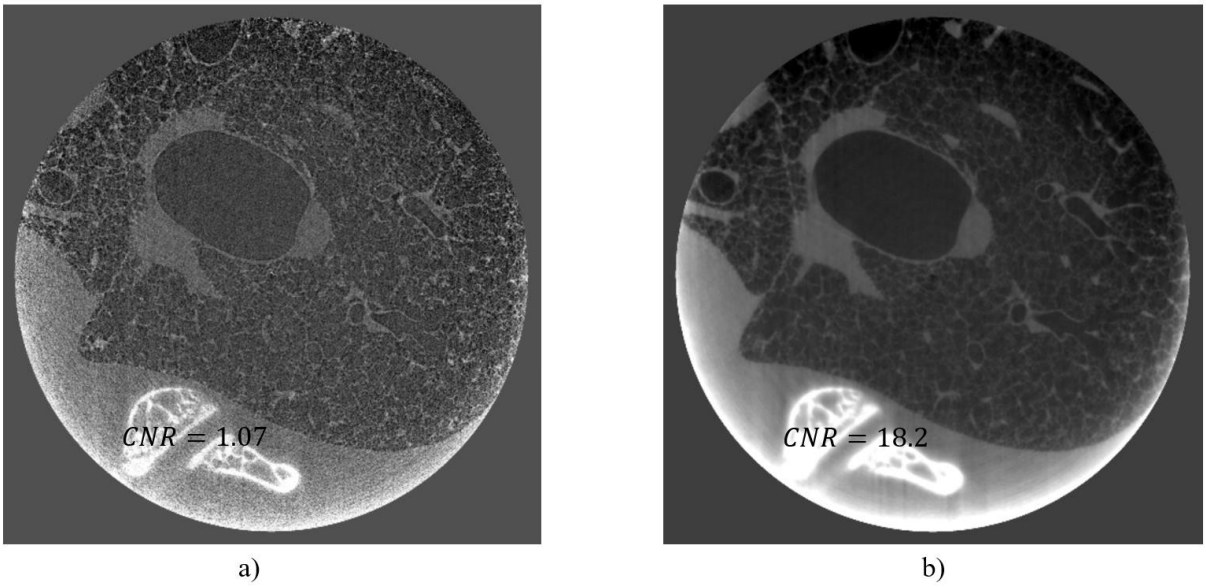

Figure 9. a) A tomographic slice with attenuation contrast reconstructed with the SIRT algorithm and b) the same slice treated with phase retrieval prior to reconstruction. The CNR of the AC image is 1.07 and of the PR image 18.2

4.2 CNR-to-ESD ratio

In figure 10 eight images are shown of one slice all being reconstructed with the Gridrec algorithm and with the application of phase retrieval. The only difference between the images is that they have been reconstructed with a decreasing number of projection angles were the first image included all the projection angles, the second kept every second, the third kept every third and so on. It can be seen that periodic stripes appear and become more and more visible as the number of used projections decrease. Figure 11 shows the corresponding slices reconstructed with the SIRT-algorithm. The degradation and appearance of artifacts is clearly visible from the image with 180 projection angles and below.

Table 1 shows the calculated CNR:s and the ESD together with the ratio, for the Gridrec-images of the different number of used projections. In table 2 the CNR and CNR-to-ESD ratios from the SIRT-images are presented.

Figure 12 shows the plot of the CNR-to-ESD ratio as a function of number of projection angles. A possible plateau can be observed in the region up to approximately 400 projection angles. The plot of the CNR-to-ESD as a function of number of used projections is shown in figure 13. As for the case with the Gridrec images a plateau is spotted up to approximately 400 projection angles.

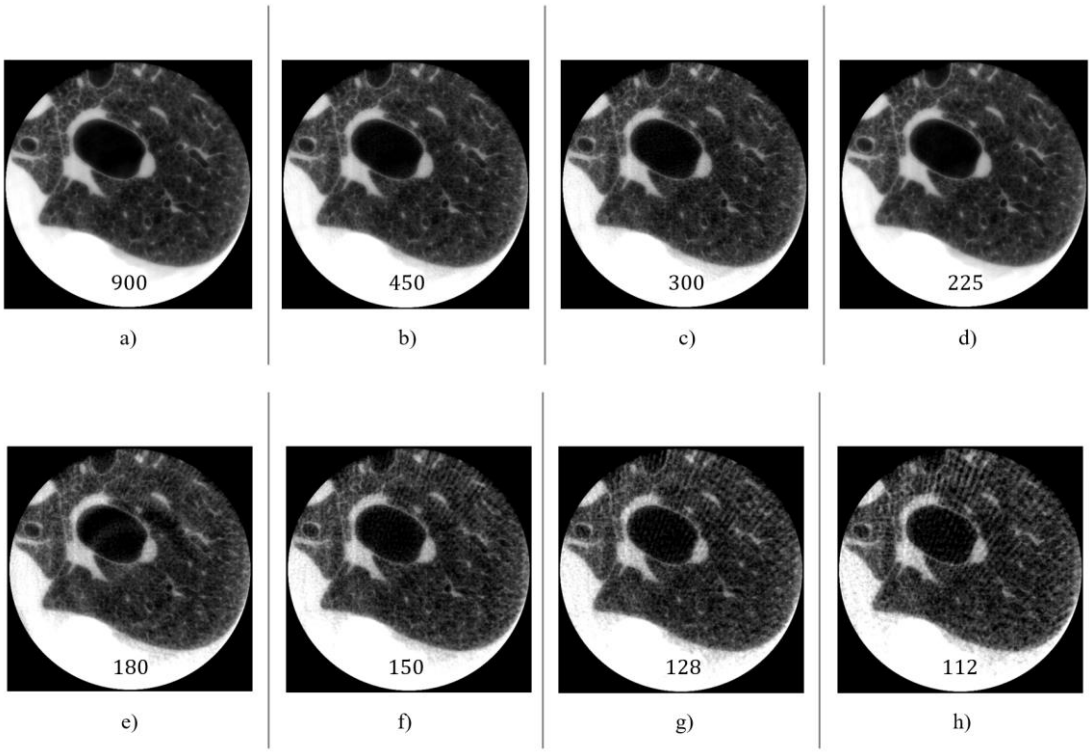

Figure 10. One slice of the tomographic data, the reconstruction have been done with Gridrec and with the application of PR. The number of projections used in the reconstructions have been varied as the following a) 900, b) 450, c) 300, d) 225, e) 180, f) 150, g) 128 and h) 112

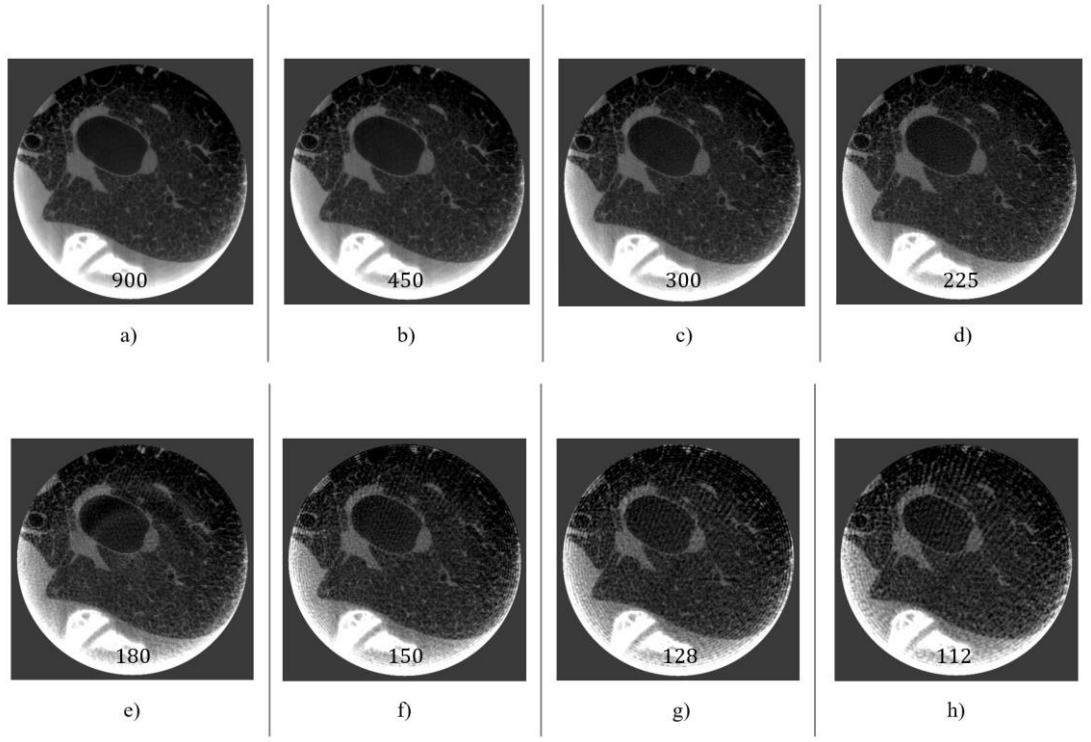

Figure 11. One slice of the tomographic data, the reconstruction have been done with SIRT and with the application of PR. The number of projections used in the reconstruction have been varied as the following a) 900, b) 450, c) 300, d) 225, e) 180, f) 150, g) 128 and h) 112

Table 1. The calculated CNR and ESD together with ratio in relation to the varied number of projection angles for the Gridrec images.

Number of projection	**CNR**		**ESD** [GY]	**CNR/Dose**	
	Center ROI	Corner ROI		Center ROI	Corner ROI
900	47.1	34.0	21.0	2.24	1.62
450	30.6	28.2	10.5	2.92	2.69
300	24.3	24.8	7.00	3.47	3.55
225	18.4	16.4	5.25	3.51	3.13
180	12.0	16.8	4.20	2.86	4.01
150	12.0	10.5	3.50	3.43	3.01
128	8.54	9.14	2.99	2.86	3.06
112	8.60	9.13	2.61	3.29	3.49

Table 2. The calculated CNR and ESD together with ratio in relation to the varied number of projection angles for the Gridrec images.

Number of projection	**CNR**		**ESD** [GY]	**CNR/Dose**	
	Center ROI	Corner ROI		Center ROI	Corner ROI
900	18.2	–	21.0	0.877	–
450	13.0	–	10.5	1.24	–
300	9.32	–	7.00	1.33	–
225	6.81	–	5.25	1.30	–
180	6.33	–	4.20	1.51	–
150	5.37	–	3.50	1.53	–
128	3.64	–	2.99	1.22	–
112	3.73	–	2.61	1.43	–

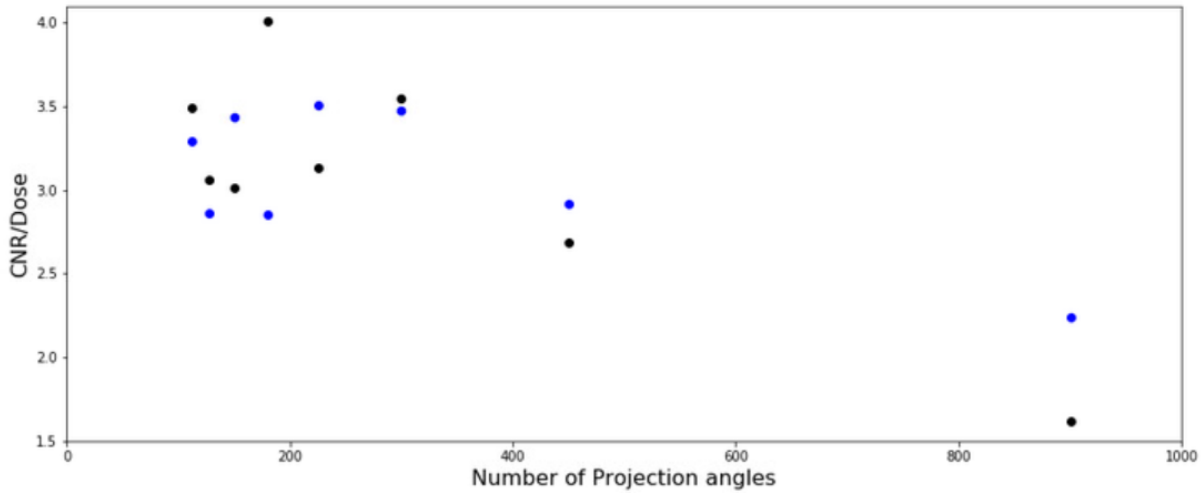

Figure 12. The CNR-Dose ratio as a function of number of projection angles. Blue dots represent the values obtained from placement of the analytical ROIs in the center of the image while the black dots are the values obtain from a ROI placed in the corner of the image.

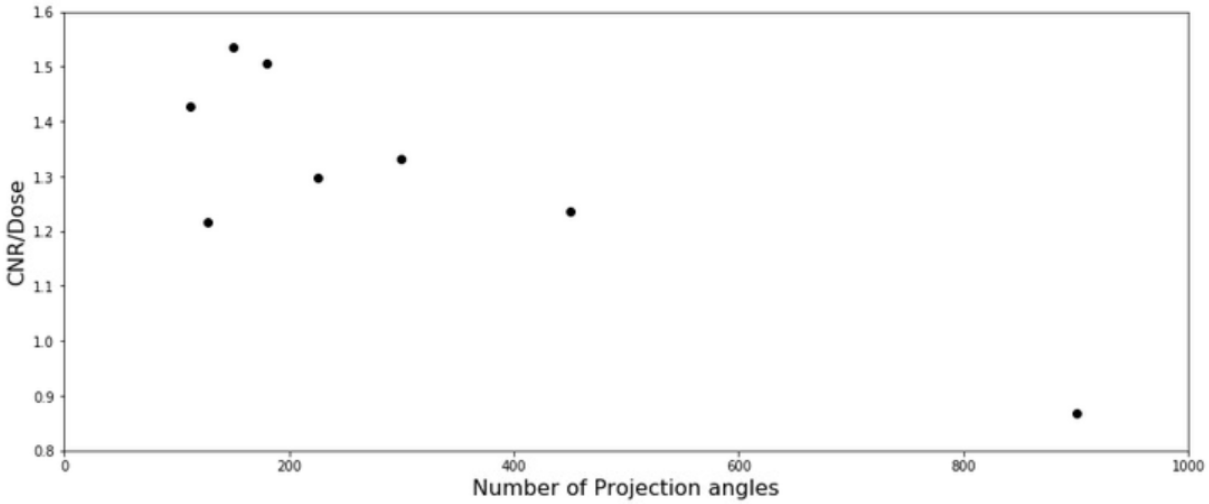

Figure 13. The CNR-Dose ratio as a function of number of projection angles.

5. Discussion

5.1 PR-AC comparison

From the results visible in figures 8 and 9 it is safe to say that the phase contrast images are advantageous over attenuation contrast images in regards of image quality (CNR) which was also shown by [1]. This is at least the case when the requirements for propagation-based phase contrast are fulfilled i.e. the X-rays are monochromatic and the propagation distance chosen correctly. The propagation-based phase retrieval algorithms require input parameters as described in section 3.2.2. While pixel size, propagation distance and photon energy are parameters that can be determined exactly, or at least with very high accuracy, the alpha-parameter cannot. The alpha-parameter, which is the ratio of the complex and real parts of the complex refractive index of the medium as described in equation (20), depends on the composition of the object. Since an object is rarely homogenous it is extremely difficult to make a decent approximation of the complex refractive index. Although an alpha-value was approximated for the mouse sample the phase retrieved images with this value wasn't the optimal one. Therefore, the alpha value was adjusted several times before reaching the optimal phase retrieval as was mentioned in section 3.2.2.

As for the CNR of the phase contrast images compared between the two algorithms the somewhat lower value for the SIRT-images could be due to various reasons one important however, is that no padding have been applied to remove the gradient over the FoV in the SIRT-reconstructions while it has been done in the Gridrec reconstructions. Therefore, the lower CNR in the SIRT- PR-image compared to the corresponding Gridrec image is reconstruction-related rather than being due to poorer combability with the phase retrieval algorithm.

5.2 Image quality-to-dose ratio

The investigation of the main objective showed that there's not only one, but rather a plateau over an interval of several number-of-projection-angles that has the highest image quality-to-dose ratio. This was observed from both the Gridrec and SIRT-images (figures 12 and 13 respectively). While the observations speak clearly in the regards that projection angles up to approximately 400 give the highest CNR-to-ESD ratio it must be taken into consideration that *CNR* is not the only metric for image quality. Furthermore, CNR as a measure of image quality has limitations nonetheless, in relation to spatial resolution. Degradation of the spatial resolution of an image results in reduced noise, [16-17] while the mean value of a certain region of the image may be unaltered. What this means for the CNR (equation [30]) is that it might be improved as the spatial resolution is degraded. The images from the decreasing number of projection angles, within the region of the plateau, may not be usable due to way too poor resolution since resolution decreases with decreasing dose (dose decreases with decreasing number of projections). For the investigation of these aspects, spatial resolution and segmentability as measures of image quality can be used. There are a number of methods

available to calculate spatial resolution, the simplest and most straightforward is taking a line profile measurement to determine the spatial resolution. Segmentability measures how well an image may be segmented - separate lung tissue from air. The way to go would be to use some segmentation method such as e.g. thresholding and evaluate (by visual inspection) how well the tissue is separated from the air.

Typically, analysis of the synchrotron-based lung images includes local air thickness analysis and curvature analysis of the individual alveoli [2]. However, these analyses are impossible to perform unless a successful binarization has been done to the images. Poor image resolution will result in loss of the thin walls between the alveoli in the segmentation step thus, leading to clumped structures i.e. a failed segmentation. Therefore, a further investigation of the possibility of segmenting the images within the plateau-region must be conducted to determine if they are usable even if the observations suggests that they have the highest CNR-to-ESD ratio.

6. Conclusions

Regarding the subobjective it can be concluded that in-line phase contrast indeed is advantageous over attenuation contrast in regards of image quality when the requirements for propagation-based phase contrast are fulfilled and all required parameters for the phase retrieval are known. However, since the composition of an object is rarely uniform the information about the complex refractive index is approximate. Thus, the alpha parameter, as described in section (3.2.2) must be adjusted to get the best possible phase contrast.

The results in figures 12 and 13 shows rather clearly that the highest CNR-to-ESD ratio is given from images generated with projection angles up to approximately 400. When increasing the number of projection angles further the gain in CNR does not increase as much as the ESD. However, this discovery does not conclude that all (or any of) the images within the region of plateau are usable. Synchrotron-based lung images require a successful segmentation prior to analysis. In the region of lower numbers of projection angles of the plateau the resolution is severely worsened. Thus, a successful segmentation might not be possible. For this reason, a further study of the segmentation possibilities of the images in the plateau region must be conducted.

7. Acknowledgements

I want to address my great gratitude to my supervisor Rajmund Mokso for all the help, support and for bearing with me considering that he had to make a lot of room for supervising me during his most busy moths of the year. I also want to address my great gratitude to my family and closest of friends for the continuous and never-ending support. But most of all AlhamduLillah.

8. References

[1] Kitchen M.J, Buckley G.A, Gureyev T.E, Wallace M.J, Andres-Thio N, Uesugi K et. al. CT dose reduction factors in the thousands using X-ray phase contrast. Scientific reports. 2017:7

[2] Lovric G, Vogiatzis Oikonomidis I, Mokso R, Stampanoni M, Roth-Kleiner M, Schittny J.C. Automated computer-assisted quantitative analysis of intact murine lungs at the alveolar scale. PLoS One. 2017 Sep 21;12(9)

[3] Lovric G, Mokso R, Arcadu F, Vogiatzis Oikonomidis I, Schittny J.C, Roth-Kleiner M et al. Tomographic in vivo microscopy for the study of lung physiology at the alveolar level. Scientific reports. 2017:7

[4] V. Nikitin, M. Carlsson, F. Andersson and R. Mokso, "Four-dimensional tomographic reconstruction by time domain decomposition," in *IEEE Transactions on Computational Imaging*.

[5] Howells M.R, Hitchcock A.P and Jacobsen C.J. Introduction: Special issue on radiation damage. Journal of Electron Spectroscopy and Related Phenomena, 170(1-3):1–3, March 2009.

[6] Howells M.R, Beetz T, Chapman H.N, Cui C, Holton J.M, Jacobsen C.J et. al. An assessment of the resolution limitation due to radiation-damage in X-ray diffraction microscopy. Journal of Electron Spectroscopy and Related Phenomena, 170(1-3):4-17, March 2009.

[7] Cotte M, Genty-Vincent A, Janssens K, Susini J. Applications of synchrotron X-ray nano-probes in the field of cultural heritage. Comptes Rendus Physique. 2018 november; 19 (7): 575-588

[8] Helgason, S. (1999). *The Radon transform*. Boston: Basel.

[9] A. C. Kak and Malcolm Slaney, *Principles of Computerized Tomographic Imaging*, Society of Industrial and Applied Mathematics, 2001

[10] Burvall, Anna & Lundström, Ulf & A C Takman, Per & Larsson, Daniel & M Hertz, Hans. (2011). Phase retrieval in X-ray phase-contrast imaging suitable for tomography. Optics express. 19. 10359-76. 10.1364/OE.19.010359.

[11] K. A. Nugent, “Coherent methods in the X-ray sciences,” Adv. Phys. 59, 1–99 (2010)

[12] ICRP, 2007. The 2007 Recommendations of the International Commission on Radiological Protection. ICRP Publication 103. Ann. ICRP 37 (2-4).

[13] Lovric G. In-vivo study of lung physiology with dynamic synchrotron-based tomographic microscopy [dissertation on the internet]. Zurich: 2015 [cited 2019 May 20]. Available from: https://lu.app.box.com/s/jlmx2hv2viciywcp4md989a4coynbwdx

[14] Paganin D, Mayo SC, Gureyev TE, Miller PR, Wilkins SW. Simultaneous phase and amplitude extraction from a single defocused image of a homogeneous object. J Microsc. 2002 Apr;206(Pt 1):33-40.

[15] *Pulmonar alveolus*. Image, viewed 2 June 2019 available at: <https://upload.wikimedia.org/wikipedia/commons/4/46/Alveolus_diagram.svg>.

[16] Brookes R. and di-Chiro G. Statistical limitations in x-ray reconstructive tomography. Medical Physics Vol 3, No 4 July 1976.

[17] Riederer S.J., Pelc N.J. and Chesler D.A. The Noise Power Spectrum in Computed Tomography Physics in Medicine and Biology 1978 23(3), 446-454.